PCCP

PAPER

View Article Online
View Journal | View Issue

Published on 25 January 2019. Downloaded by National Synchrotron Radiation Research on 1/9/2020 4:44:22 AM.

Check for updates

Cite this: *Phys. Chem. Chem. Phys.*, 2019, **21**, 3960

Solution properties of imidazolium-based amphiphilic polyelectrolyte in pure- and mixed-solvent media†

Chien-You Su,[a] Han-Liou Yi,[a] Li-Duan Tsai,[b] Ming-Chou Chen*[c] and Chi-Chung Hua*[a]

Received 13th November 2018,
Accepted 25th January 2019

DOI: 10.1039/c8cp07027j

rsc.li/pccp

The solution properties of a synthesized imidazolium-based amphiphilic polyelectrolyte dissolved in pure- and mixed-solvent media composed of two aprotic polar solvents (*N*,*N*-dimethylacetamide (DMAc) and *N*-methyl-2-pyrrolidone (NMP)) having a similar dielectric constant are explored in the semidilute regime (1–4 wt%). Rheological characterizations reveal that the use of mixed-solvent media (*e.g.*, DMAc/NMP with 1 : 1 in volume fraction, designated as 1 : 1 DMAc/NMP) leads to a substantial reduction in the solution viscosity while altering the fluid attribute from gel-like ($G' > G''$) to critical-gel-like ($G' \sim G'' \sim \omega^n$, with $n \cong 0.5$). To gain insight into these peculiar rheological features, dynamic light scattering analysis of the representative 1 : 1 DMAc/NMP medium indicates that the fraction and mean hydrodynamic radius of the micrometer-sized cluster alter substantially, too. Multiscale static light/X-ray scattering characterizations further reveal that only the NMP and 1 : 1 DMAc/NMP media (and not the DMAc) are capable of producing hierarchical structures of the cluster interior that are beneficial to mesoscale ion conduction, as supported by ac conductivity measurements. Overall, the present findings suggest that an appropriate selection of mixed-solvent media may offer an exceptional opportunity to promote the rheological, structural, and ion-conduction properties of a polyelectrolyte solution beyond the reach of the corresponding pure-solvent media.

Introduction

Anion exchange membranes (AEMs) made of functionalized polyelectrolytes have currently received much attention for fuel cell applications owing to low catalyst cost, high fuel flexibility, and less corrosion concern.[1–4] With increasing content of ionic groups in the design of existing polyelectrolytes to compensate for the inherently low mobility of hydroxide ions (OH^-), the consequent weakening both in dimensional and mechanical stability of an AEM becomes a critical concern in view of water uptake and membrane swelling.[5] To resolve this dilemma, (physical) cross-linking among the polyelectrolyte molecules, especially the formation of (local or global) interpenetrating polymer network (IPN),[6,7] has become the working principle to strengthen the mechanical properties of AEMs while producing fair OH^- conductivity.[1,4] Recently, there has been breakthrough in controlling the formation of efficient ion-conducting channels through hydrophilic/hydrophobic separation and the resulting aggregates (or clusters) of suitable size. This strategy has been shown to greatly improve the OH^- mobility while maintaining low membrane swelling,[5,8–18] by means of optimization in the chemical structure of polyelectrolytes (*e.g.*, introducing hydrophobic[8,9,19,20] or hydrophilic[10] side chains).

To date, (generally poor) solution-processability has posed an additional challenge in producing high-performance cross-linked AEMs through large-area membrane casting.[21] This situation has been greatly improved by the recent success in synthesizing solution-processable ionic copolymers,[22,23] which have motivated the fabrication of solution-processed AEMs. The existing strategies for controlling the degree of cross-linking, however, involved raising the reaction temperature (for thermal cross-linking)[13,24,25] and exposure time of UV-light (for photo cross-linking)[26,27] after membrane fabrication. Clearly, the ability to control the cross-linking (physical or chemical) reactions in the pristine solution would offer an additional opportunity to optimize the membrane properties. This can, in principle, be achieved through precise controls over the solvent quality.[28–30] Specifically, mixed-solvent media composed of aqueous/organic mixtures have previously been shown to

[a] *Department of Chemical Engineering, National Chung Cheng University, Chia-Yi 62102, Taiwan, Republic of China. E-mail: chmcch@ccu.edu.tw*
[b] *Material and Chemical Research Laboratories, Industrial Technology Research Institute, Hsinchu 31040, Taiwan, Republic of China*
[c] *Department of Chemistry, National Central University, Jhong-Li 32001, Taiwan, Republic of China. E-mail: mcchen@cc.ncu.edu.tw*

† Electronic supplementary information (ESI) available. See DOI: 10.1039/c8cp07027j

This journal is © the Owner Societies 2019

Published on 25 January 2019. Downloaded by National Synchrotron Radiation Research on 1/9/2020 4:44:22 AM.

produce desirable solvent qualities,[31–36] as revealed in viscosity and optical-scattering characterizations for the underlying chain conformation and aggregate morphology.[33,35–38]

Herein, we describe the synthesis and preparation of a novel imidazolium-based amphiphilic polyelectrolyte dissolved in a representative series of pure- and mixed-solvent media composed of two aprotic polar solvents, *i.e.*, *N*,*N*-dimethylacetamide (DMAc) and *N*-methyl-2-pyrrolidone (NMP), having a similar dielectric constant, so that the sole impact of varying solvent quality may be unambiguously discriminated. The solution properties in the semidilute regime are systematically explored using multiscale dynamic/static analysis schemes. Rheological measurements reveal that the use of mixed-solvent media, largely independent of the actual solvent composition, leads to a substantial reduction in solution viscosity, and the fluid attribute alters from gel-like to critical-gel-like that is expected to greatly facilitate the solution processing without compromising the mechanical strength of a solution-cast membrane in future applications with AEMs. To gain insight into these peculiar rheological features, dynamic light scattering (DLS) analysis reveals the ubiquitous existence of two distinct species in the polyelectrolyte solution, namely, the nanometer-sized polyion and micrometer-sized cluster. In particular, the (volume) fraction and mean hydrodynamic size of the cluster species fostered in the representative 1 : 1 DMAc/NMP medium differ substantially from those produced in the pure-solvent media. As the presence of micrometer-sized polyelectrolyte clusters is expected to aid the mesoscale ion conduction and has rarely been reported in early work, we also perform detailed (multiscale) structural analysis from small-angle light scattering (SALS), static (wide-angle) light scattering (SLS), and small-angle X-ray scattering (SAXS). The results reveal interesting hierarchical structures for the cluster incubated in the NMP and 1 : 1 DMAc/NMP media—and not for the DMAc medium—that may serve as the highway of ion conduction within the cluster, as supported by ac conductivity measurements. The overall findings suggest that an appropriate selection of mixed-solvent media that are selectively attractive to different parts of an amphiphilic polyelectrolyte molecule may offer an exceptional opportunity to promote the rheological, structural, and ion-conduction properties of the resulting solution beyond the reach of the corresponding pure-solvent media.

Experimental section

Materials and sample preparation

The chemical structure of the polyelectrolyte molecule in this study is shown in Fig. 1 along with the two solvents used. Details of the synthesis schemes can be found in a patent application currently in progress.[39] The polyelectrolyte molecule was prepared through a ring-opening metathesis polymerization (ROMP). The polyelectrolyte molecule is composed of a cationic repeating unit with imidazolium functional group and a nonionic repeating unit with C_6 alkyl side group. The aforementioned two types of repeating units are arranged in a random fashion along the polymer backbone. The ratio

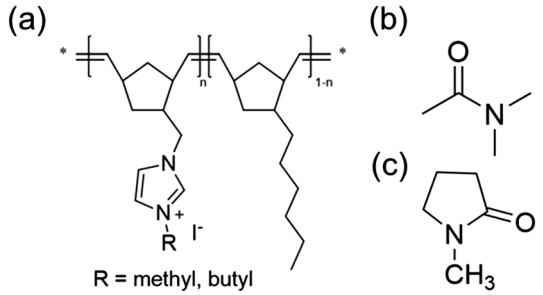

Fig. 1 Chemical structures of (a) polyelectrolyte, (b) DMAc, and (c) NMP molecules in this study.

between cationic and nonionic units was controlled to be 7 : 3, and the number-averaged molecular weight of the polyelectrolyte was estimated to be 100 000–250 000 g mol^{-1}. The solvents, DMAc (Alfa Aesar, 99% in purity) and NMP (Alfa Aesar, 99% in purity), used to prepare the polyelectrolyte solutions were filtered through a 0.22 μm PTFE Millipore filter to remove dust. The solvent mixtures were then prepared using different volume fractions of DMAc and NMP, with the actual fractions designated in the nomenclature of the resulting solution samples (*e.g.*, 1 : 1 DMAc/NMP). The 1 and 4 wt% polyelectrolyte solutions prepared with pure or mixed solvents were sonicated for 8 h at 25 °C. The solutions were then treated with a high-speed homogenizer (T25 digital ULTRA-TURRAX®, IKA, Staufen, Germany) and dispersing element (S25N-10g) operated at 20 k rpm for 1 min with a 30 s rest between two consecutive runs; no apparent polymer degradation was found in subsequent viscosity characterizations. Unless stated otherwise, the 4 wt% solutions are utilized in viscometric characterizations to mimic the conditions of membrane fabrication, while the 1 wt% solutions are investigated throughout this work for their ability to produce fair-quality scattering (dynamic and static) data on semidilute polyelectrolyte solutions that are of practical and scientific interest.

Rheological measurements

Rheological measurements were performed using a stress-controlled rheometer (DHR-2, TA Instruments) that is equipped with a cone-and-plate fixture (diameter = 40 mm, cone angle = 2°) and solvent trap. All measurements were conducted at 25.0 ± 0.1 °C, including rotation and oscillation experiments. Fair consistency between data obtained using different fixtures helped validate the data reported herein. In the rotation experiment, startup of steady shear experiment was performed at several constant shear rates ranging from 0.1–800 s^{-1}, with the steady viscosity at a given shear rate determined from the time-averaging of the long-time data. In the oscillation experiment, frequency sweep was carried out with angular frequencies ranging from 0.1 to 300 rad s^{-1} at a constant strain of 0.1, which has been identified to fall in the linear viscoelastic (LVE) region by the results of amplitude-sweep experiment operated at an angular frequency of 10 rad s^{-1}.

Light scattering (SLS/DLS) analyses

Light scattering (LS) measurements were performed on a laboratory-built apparatus as described elsewhere.[40,41] A 34 mW

Published on 25 January 2019. Downloaded by National Synchrotron Radiation Research on 1/9/2020 4:44:22 AM.

polarized He–Ne laser (λ_0 = 632.8 nm; Lasos, LGK 7626S) was used as the incident light. The vial containing the sample solution of 2 mL in volume is a cylindrical quartz cell with 1 cm in diameter (Hellma, 540.111, Germany); a cap is utilized to prevent solvent evaporation during the entire experiment. All measurements were conducted at 25.0 ± 0.1 °C for a range of scattering angles θ = 30–140°. Details of SLS and DLS analysis schemes can be found in prior work.[40–42]

Small-angle scattering (SALS/SAXS) analyses

SALS measurements may complement the usual SLS experiment in exploring large aggregate clusters that bear characteristic sizes falling in the micrometer range, as is essential in this study. The setup of the SALS apparatus was described elsewhere.[41] A 2 mW He–Ne laser with a wavelength of λ_0 (= 632.8 nm) and beam diameter of 0.8 mm was used as the incident light, which was guided through a spatial filter to enhance beam homogeneity. Data were collected in a range of scattering angles θ = 0.7–20°. SAXS measurements were carried out at beamline station BL23A of Taiwan Light Source (TLS) at the National Synchrotron Radiation Research Center (NSRRC) in Taiwan. The scattering X-ray covers a q-range of 0.04–3.2 nm^{-1}, with 15 keV incident beam (wavelength l_0 = 0.827 Å) and sample-to-detector distance of 4352 mm. All measurements were conducted at 25.0 ± 0.1 °C.

AC conductivity analysis

Ac conductivity measurements were performed using a Solartron 1296 dielectric interface coupled to a Solartron 1260 frequency response analyzer, operated in the range of frequencies 10^{-2}–10^{4} Hz with a small voltage (100 mV) in the linear impedance region. The sample was placed between parallel-plate electrodes (diameter = 25 mm and gap size = 1 mm) made of stainless steel and electrically insulated with machining ceramics, along with a laboratory-built temperature controller. All experiments were conducted at 25.0 ± 0.1 °C.

Results and discussion

Rheological features

The solution viscosity as a function of shear rate for a representative set of 4 wt% polyelectrolyte solutions with varying solvent composition is shown in Fig. 2a; the measured solvent viscosities for DMAc and NMP using the Cannon-Fenske viscometer are 0.99 and 1.79 cP, respectively, in close agreement with the results reported in the literature.[43,44] All solutions in this study exhibit pronounced shear-thinning behavior within the range of shear rates investigated. A salient feature is that the solutions prepared with mixed solvents generally yield a much lower viscosity than those prepared with pure solvents. In particular, the use of the 1 : 1 DMAc/NMP medium can be seen to result in an about tenfold decrease in the solution viscosity. In semidilute polyelectrolyte solutions, the variation in solution viscosity was often ascribed to the so-called clustering effect or strength,[45] which arises from the polyion associations

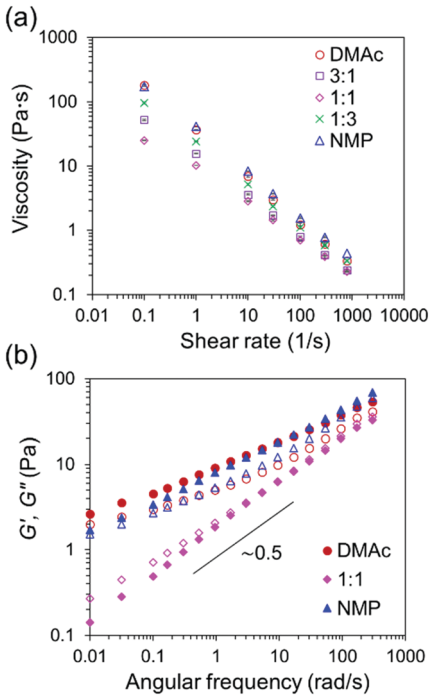

Fig. 2 (a) Solution viscosity as a function of shear rate and (b) dynamic modulus responses, G' (solid symbols) and G'' (open symbols), as functions of the angular frequency for the 4 wt% polyelectrolyte solutions prepared with various volume fractions of DMAc and NMP. The measured viscosities for the five solvent media are 0.99, 1.17, 1.39, 1.58, and 1.79 cP with decreasing DMAc content.

that balance electrostatic and entropic forces. The DLS analysis discussed shortly suggests that the pronounced reduction in solution viscosity as has been observed here bears an origin of altered polyion/cluster partition and mean cluster size in the mixed-solvent media.

Fig. 2b further compares the results from dynamic frequency sweep on the solutions prepared with DMAc, 1 : 1 DMAc/NMP, and NMP. Given that a similar trend has been noted with the 1 : 3 and 3 : 1 DMAc/NMP media, as shown in Fig. S1 (ESI†), subsequent discussions will be focused on this particular set of polyelectrolyte solutions. For the two pure-solvent systems, the trend $G' > G''$ applies and is indicative of elastic or gel-like behavior; the pronounced frequency dependence for G' is reminiscent of weak gels (*cf.*, $G' \sim \omega^0$ for strong or hard gels). A distinct trend $G' \sim G'' \sim \omega^n$, with $n \cong 0.5$ is observed, however, for the 1 : 1 DMAc/NMP polyelectrolyte solution, in addition to a substantially reduced strength of dynamic modulus. The above viscometric feature has been associated with critical gels near (yet below) the gel point (*i.e.*, $G''/G' = 1$).[46] Together with the solution viscosities presented in Fig. 2a, it should be clear that the use of mixed-solvent media can have a profound impact on the rheological properties of the polyelectrolyte solutions investigated. In fact, the critical-gel behavior noticed for the 1 : 1 DMAc/NMP medium often represents an advantageous one to warrant a fair solution processability without compromising the desirable elasticity of the solution-cast membrane.

 This journal is © the Owner Societies 2019

Published on 25 January 2019. Downloaded by National Synchrotron Radiation Research on 1/9/2020 4:44:22 AM.

For polyelectrolyte solutions without salt addition, early studies have revealed that the formation of polymer clusters, including their structure and size, is sensitive to the effects of solvent quality[47] and dielectric constant.[48] Given that there is an only slight difference in the dielectric constants for DMAc (ε_r = 37.80 at 298 K[49]) and NMP (ε_r = 32.17 at 298 K[50]), this particular factor should play minor roles in this study and, therefore, the impact of solvent quality can be discriminated. The following (dynamic and static) scattering analyses suggest, however, that the impact of solvent quality for the polyelectrolyte solutions investigated is manifold and "multiscale" in nature, as it cannot be explained by any single attribute often regarded as a manifestation of solvent quality (*e.g.*, the coil size, the population, size, and structural compactness of an aggregate species).

Dynamic light scattering analyses

Fig. 3 presents the field autocorrelation function, $|g^{(1)}(q,t)|$, and the associated decay time distribution, $G(t) = G(1/\Gamma)$ (Γ being the decay rate), for the 1 wt% polyelectrolyte solutions. For the cases with NMP and 1 : 1 DMAc/NMP media, three relaxation modes may be identified, all exhibiting a diffusive attribute (*i.e.*, $\Gamma \sim q^2$). The overall feature for the DMAc medium is basically no different, except for the absence of the second (intermediate) mode. Note that, in addition to the characteristic diffusional motion associated with each relaxation mode, Fig. S2a (ESI†) demonstrates for the case of the first (fast) mode that the existence of an individual relaxation mode may be confirmed by scrutinizing the curve fittings that include or exclude the contribution of a particular mode. The significance of the apparent absence of the second (intermediate) mode for the DMAc medium will be further discussed in a later structural analysis. For comparison, Fig. S2b–d (ESI†) shows that similar DLS features can be found for the dilute (0.1 wt%) counterparts.

The estimated R_H for the three relaxation modes listed in Table 1 fall approximately in the ranges of 1 nm, 100 nm, and >1 μm, respectively. The first (fast) and third (slow) modes resemble the ones reported in prior DLS studies on polyelectrolyte solutions,[51–54] except for the (micrometer) size of the slow-mode species. The fast mode in previous studies was often attributed to the collective diffusion of counterions and polyions, and the slow mode was assigned to the aggregate clusters—either in the form of temporal aggregates[52] or multichain domains.[54,55] The second (intermediate) mode was occasionally reported with polyelectrolyte blend solutions[53] and amphiphilic copolymer solutions.[56,57] In the present DLS analysis, the three relaxation modes are henceforth referred to as polyion, aggregate, and (micrometer-sized) cluster, respectively.

To know the population of each species in a polyelectrolyte solution, the approximate volume fraction (W_i) for each species is estimated using the intensity-weighted DLS area (w_i) as $W_i = \left(w_i/R_{H,i}^2\right) \Big/ \sum_i \left(w_i/R_{H,i}^2\right)$,[42,58–60] with the results listed in Table 1. In the previous formula, the scattering intensity may be rescaled with the square (for Gaussian coils)[59] or cubic (for solid spheres)[60] of the mean hydrodynamic radius, $R_{H,i}$, and the results seem to be insensitive to either assumption made. Several important features in Table 1 can be noted. While the mean (apparent) size of the polyion species (*i.e.*, the fast mode) exhibits little dependence on the solvent medium used, the mean cluster size alters substantially, with the 1 : 1 DMAc/NMP medium fostering the smallest among the three. Additionally, the population ratio of polyion/cluster is the highest for the same medium. Together with the prior rheological features in Fig. 2, it is significant to observe that the

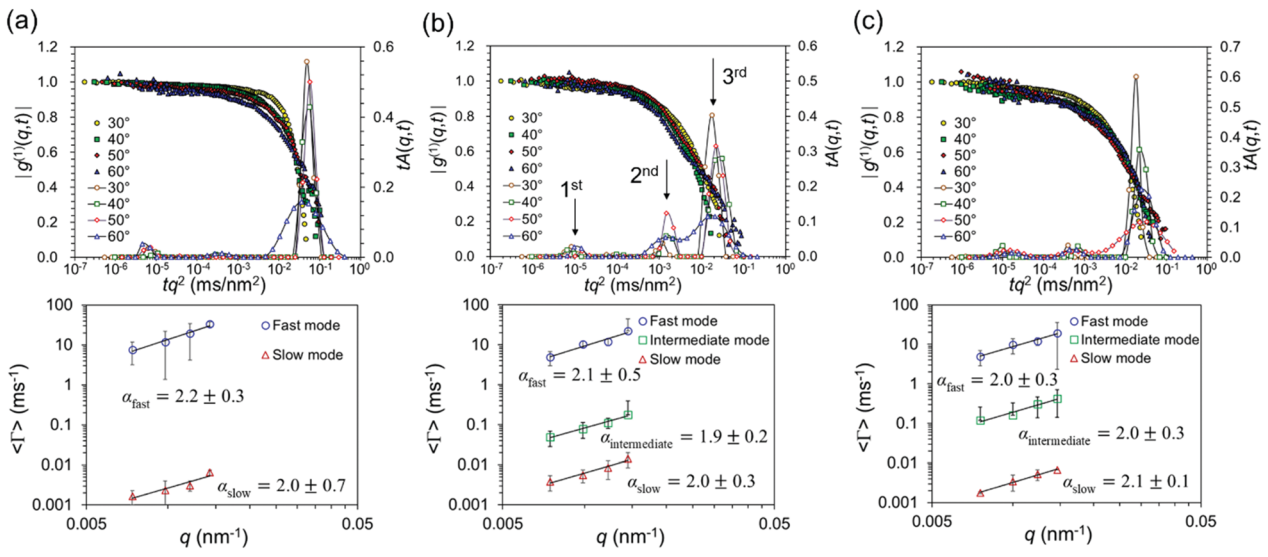

Fig. 3 Angular dependences of the field autocorrelation function and the associated decay time distribution extracted from CONTIN for the 1 wt% polyelectrolyte solutions prepared with (a) DMAc, (b) 1 : 1 DMAc/NMP, and (c) NMP, where the decay time t has been rescaled with q^2. The arrows in (b) designate three relaxation modes representing polyion, aggregate, and cluster, respectively. The mean decay rate, $\langle\Gamma\rangle$, as a function of scattering vector q is shown in the bottom to demonstrate the diffusive attributes of all three relaxation modes.

Published on 25 January 2019. Downloaded by National Synchrotron Radiation Research on 1/9/2020 4:44:22 AM.

Table 1 Parameter values extracted from the DLS analysis on the 1 wt% polyelectrolyte solutions prepared with three representative solvent media[a]

Solvent	$R_{H,ion}$ (nm)	$R_{H,agg}$ (nm)	$R_{H,cluster}$ (nm)	W_{ion} (%)	W_{agg} (%)	$W_{cluster}$ (%)	Ion-to-cluster ratio
DMAc	1.6 ± 0.1	n/a	8200 ± 800	43	0	57	0.75
1:1	1.7 ± 0.1	202 ± 7	2600 ± 130	83	5	12	6.92
NMP	1.5 ± 0.1	66 ± 3	4000 ± 100	72	1	27	2.67

[a] The mean volume fractions, W_i, denote the values evaluated from data on the smallest scattering angle $\theta = 30^\circ$ in this study. The "ion" in this table denotes the abbreviation of "polyion".

1:1 DMAc/NMP medium is capable of modifying both the population and size of the cluster species in a way that cannot be achieved by either of the pure-solvent media. Accordingly, the general trends noticed in Fig. 2 may be explained by the fact that the 1:1 DMAc/NMP medium helps produce the smallest partition and mean size for the cluster species. From this perspective, the 1:1 DMAc/NMP medium seems to bear the best solvent quality among all three solvent media under consideration. Later, we discuss a different perspective of solvent quality that leads to a slightly different conclusion as has been reached here on the basis of rheological and DLS characterizations.

It is worth noting that only a few experimental[47,61,62] and computational[63] studies to date have demonstrated similar (peculiar) effects of mixed solvents for amphiphilic polymers. The reentrant coil-to-globule-to-coil transition first reported by Zhang and Wu[61,62] for ultralong linear poly(*N*-isopropylacrylamide) (PNIPAM) in water/methanol media represents a renowned example showing that the mixture of two good solvents may result in a much poorer medium due to the formation of various types of water–methanol complexes. Clearly, for the polyelectrolyte solutions investigated herein, we seem to report on a distinct type of reentrant phenomenon, wherein two poorer solvents combine to form better solvent media in view of the viscometric and DLS features discussed earlier. The underlying physics is believed to differ substantially, too, as DMAc and NMP show no tendency to form complexes, and even if they do, the solvent quality is expected to worsen rather than improve. In fact, the structural analysis discussed next and the absorption spectra shown in Fig. S3 (ESI†) both suggest that the (local) solvation behavior[64] and the resulting polyelectrolyte conformation alter in various solvent media, and the implied solvent quality for the 1:1 DMAc/NMP medium falls somewhere in between those of the two pure-solvent media and, therefore, cannot explain the peculiar viscometric features seen in Fig. 2. Our conjecture is that the pronounced reduction in the solution viscosity associated with the mixed-solvent media (Fig. 2a) likely stems from the solvent-mediated (bulk) aggregation state—including both the population and size of the cluster species, as explained earlier. This notion can also explain while the low-frequency dynamic modulus responses (which are sensitive to the bulk aggregation state) in Fig. 2b alter substantially for the 1:1 DMAc/NMP medium, the corresponding high-frequency responses (which reflect mainly the local aggregation properties and chain conformation) differ only slightly among the three solvent media. In this respect, a recent simulation study on two representative binary-solvent systems for a conjugated polymer, MEH-PPV (poly(2-methoxy-5-(2′-ethylhexyloxy)-1,4-phenylenevinylene)), was especially instrumental in revealing how the synergic effects of two distinct solvent species that are selectively attractive to different parts of the polymer can lead to exceptional conformational properties beyond the reach of either solvent medium,[63] in accord with the experimental findings on the corresponding thin-film performance.[65,66] In either case, however, it remains to be clarified how the altered solvent quality prevails to eventually modify the bulk aggregation state in a way that cannot be fully predicted on the basis of single-chain properties.

Multiscale structural characterizations

Resolving the geometrical and structural features of the (micrometer-sized) cluster and polyion species requires scattering intensity profiles that cover a wide q-range. Presently, SAXS[67] (q = 0.04–3 nm^{-1}), SLS (q = 0.007–0.03 nm^{-1}), and SALS (q = 0.0001–0.005 nm^{-1}) measurements are combined to meet this requirement. Fig. 4 presents the combined SALS/SLS/SAXS profiles, which effectively cover length scales of about five orders of magnitude. To resolve the multiscale structures manifested by the scattering data in Fig. 4, the following formulations are utilized:

$$I(q) = I_{cluster}(q) + I_{agg}(q) + I_{chain}(q) \quad (1)$$

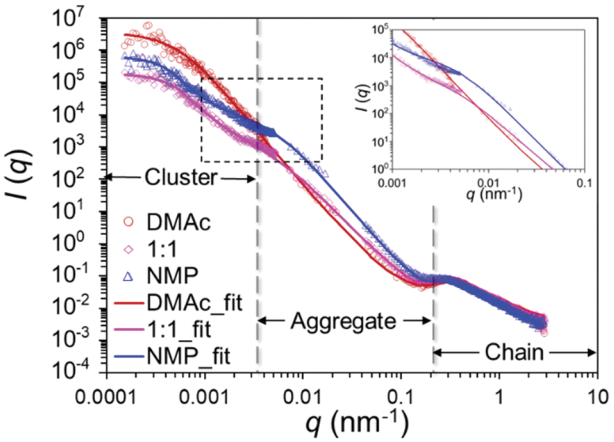

Fig. 4 Combined SALS/SLS/SAXS intensity profiles for the 1 wt% polyelectrolyte solutions prepared with DMAc, 1:1 DMAc/NMP, and NMP, where the SALS and SLS data have been vertically shifted to warrant a smooth transit to the absolute SAXS data. The vertical dashed lines mark three distinct structural regions, as suggested by prior DLS analysis. The inset presents the magnified figure for the region marked by the dashed square.

Published on 25 January 2019. Downloaded by National Synchrotron Radiation Research on 1/9/2020 4:44:22 AM.

with

$$I_{\text{chain}}(q) = k_1 S_{\text{electrostatic}}(q) P_{\text{wormlikechain}}(q)$$

$$I_{\text{agg}}(q) = k_2 S_{\text{fractal}}(q) P_{\text{packing}}(q)$$

where k_i is a constant factor. The structure and form factors employed in the fitting can be found in the ESI.†

Briefly, $I_{\text{chain}}(q)$in the high-q region denotes the contribution of isolated polyelectrolyte chains, which may be described by the wormlike chain model ($P_{\text{wormlikechain}}(q)$)[68–70] along with an electrostatic structure factor ($S_{\text{electrostatic}}(q)$).[68] Except for the DMAc medium, $I_{\text{agg}}(q)$ in the intermediate-q region can be seen to harbor a secondary structure (*i.e.*, a plateau region) at low q, indicative of the existence of (mesoscale) building units or aggregates within the (micrometer-sized) cluster. The scattering intensity in this region may be described by the product of a structural factor describing the mass-fractal structure of the aggregate interior and a form factor for the constituting polyelectrolyte chains. The contribution from the cluster species, $I_{\text{cluster}}(q)$, in the low-q region may be described by the Guinier–Porod model,[71] which captures the size and (interior) mass-fractal structure of an average cluster. For the DMAc system, which lacks the aggregate species in prior DLS analysis and a secondary structure as noted above, the same formula for "$I_{\text{agg}}(q)$" may be employed to fit the scattering data that cover the "aggregate" and "cluster" regions. In this case, it is important to note that the structural parameters shown in Table 2 denote the properties of the entire cluster species. Given that depolarized DLS (*i.e.*, DDLS) analysis reveals no discernible signals that would suggest the presence of anisotropic species (ESI,† Fig. S4), the present model fits need to consider only standard formulas for isotropic species, and it is evident that the main results reported herein should be largely independent of the particular models and fitting strategies adopted. For more detailed comparisons, the model fits that show the contribution from the individual species as well as the compilation of a full set of fitted parameters can be found in Fig. S5 and Table S1 (ESI†).

In the "chain" regime, the persistence length (l_p) for a polyelectrolyte molecule reflects the dual effect of intrinsic chain flexibility and segmental electrostatic interactions,[68,69,73] and the results in Table 2 indicate a slight influence of solvent quality on this particular (local) quantity. Besides, the contour length (l_c) is independently estimated from the known molecular weight(s) for the polyelectrolyte investigated (with the segmental length of two consecutive monomers being approximately 1.2 nm). The estimated contour length ($l_c \sim$ 300–630 nm) agrees reasonably with the fits from the wormlike chain model, which, additionally, captures the variation due to the effect of solvent quality. According to the scaling relationship discussed shortly, the polyelectrolyte chains in DMAc adopt a "bead-controlled" conformation that results in a shorter contour length, whereas the chains assume a "string-controlled" conformation in NMP and 1 : 1 DMAc/NMP and thus longer contour lengths.

In a narrow range of $I(q)$ where $I_{\text{chain}}(q)$ and $I_{\text{agg}}(q)$ intersect, a pronounced peak in the SAXS profile—the so-called polyelectrolyte peak—can be clearly identified. This characteristic feature for semidilute polyelectrolyte solutions was often attributed to the effect of long-range electrostatic interactions between polyions,[54] and the corresponding scaling law with respect to the polymer concentration may be utilized to identify a particular concentration regime[70,74] or solvent quality.[47,75] The scaling relationships between q^* (*i.e.*, the location of the polyelectrolyte peak) and polyelectrolyte concentration, $q^* \propto c_p^{\gamma}$, can be found in Fig. S6 (ESI†). The scaling exponents for DMAc, 1 : 1 DMAc/NMP, and NMP media range from 0.35 to 0.5, reminiscent of a transition in chain conformation from the bead-controlled ($\gamma \cong 1/3$) to string-controlled ($\gamma \cong 1/2$) regime within the classical pearl-necklace model.[76] Because of a similar dielectric constant for the two pure solvents, solvent quality should play a major role here. In fact, NMP has been reported to bear good solvation power for poly(norbornene)s with ionic imidazolium moieties.[77] The scaling exponent for the 1 : 1 DMAc/NMP medium implies a solvent quality somewhere in between those of the two pure solvents, as mentioned earlier. Thus, it seems that the peculiar solvent quality as implied by the results in Fig. 2 (rheological) and Fig. 3 (DLS) for this particular mixed-solvent medium cannot be captured by this conventional classification of solvent quality.

The main part of the scattering intensity (SLS/SAXS) profile in the "aggregate" regime is characterized by mass-fractal structures, with the mass-fractal dimension falling in the range of $D_{\text{m,agg}}$ = 2.6–2.9 for the three solvent media investigated. As we noted earlier, however, only the SALS profiles for the NMP and 1 : 1 DMAc/NMP media consist of a pronounced plateau in the range of $0.003 < q < 0.005$ nm^{-1}, indicative of the existence of hierarchical structures. Thus, the cluster species fostered in these two media is composed of (mesoscale) building units or aggregates, in contrast with the "featureless" (interior) structure in the DMAc medium. The mean size of the

Table 2 Structural parameters fitted from eqn (1) using the scattering intensity profiles shown in Fig. 4

Solvent	$R_{\text{g,cluster}}$ (nm)	$D_{\text{m,cluster}}$	ρ_{cluster}[a]	$R_{\text{g,agg}}$ (nm)[b]	ζ (nm)	$D_{\text{m,agg}}$	$R_{\text{g,packing}}$ (nm)	$R_{\text{g,chain}}$[c] (nm)	l_c (nm)	l_p (nm)	ξ (nm)
DMAc	4320 ± 360	2.9 ± 0.3	0.53	n/a	1793 ± 158	n/a	12.8 ± 1.1	15.1	245.0 ± 21.6	2.8 ± 0.2	7.8 ± 0.7
1 : 1	3430 ± 135	2.8 ± 0.1	1.32	521	226 ± 9	2.6 ± 0.1	11.1 ± 0.4	14.8	273.6 ± 10.8	2.4 ± 0.1	7.2 ± 0.3
NMP	4160 ± 190	2.7 ± 0.1	1.04	447	200 ± 9	2.9 ± 0.1	13.4 ± 0.6	15.3	319.0 ± 14.9	2.2 ± 0.1	7.6 ± 0.4

[a] $\rho_{\text{cluster}} = R_{\text{g,cluster}}/R_{\text{H,cluster}}$, where $R_{\text{H,cluster}}$ can be found in Table 1. [b] $R_{\text{g,agg}} = [D_{\text{m,agg}}(D_{\text{m,agg}} + 1)]^{0.5}\zeta$; for comparison, the Debye function yields results of $R_{\text{g,agg}}$ = 641 and 507 nm for the 1 : 1 DMAc/NMP and NMP media, respectively. [c] $R_{\text{g,chain}} = (l_c l_p/3)^{0.5}$, from the Sharp and Bloomfield wormlike chain model.[72]

Published on 25 January 2019. Downloaded by National Synchrotron Radiation Research on 1/9/2020 4:44:22 AM.

building aggregate, $R_{g,agg}$, estimated from the structure factor is in good agreement with that obtained from the form-factor fit using the Debye function near the plateau region (see footnotes in Table 2). To simply the fitting in the high-q region for the packing chains, the same function for a Gaussian chain is employed for $P_{packing}(q)$ in eqn (1), and the results on the mean radius of gyration, $R_{g,packing}$, are in good agreement with those estimated from $P_{wormlikechain}(q)$ in Table 2, suggesting they are of the same species. For comparison, we note that the use of spherical-particle form factor for $P_{packing}(q)$ leads to $R_{g,packing}$ that is in lesser agreement with $R_{g,chain}$.

It is also worth noting that the mean radius of gyration of the building aggregate, $R_{g,agg} \sim 500$ nm, bears the same order of magnitude as with the hydrodynamic radius of the aggregate species, $R_{H,agg} \sim 100$–200 nm, identified in the DLS analysis (see Table 1), suggesting that they might represent the same or similar species. This central implication is, in fact, consistent with the observations that the DMAc medium yields no intermediate relaxation mode in the DLS experiment and, consequently, lacks a secondary structure in Fig. 4. The absence of an intermediate (aggregate) species in the DMAc medium might be ascribed to the ''bead-controlled'' polyelectrolyte conformation that facilitates more compact chain packing throughout the entire cluster species (see also discussions below). In contrast, the ''string-controlled'' polyelectrolyte conformation fostered in the other two media helps produce stabilized, loose aggregate species that is in quasi-equilibrium with the cluster species.

In most part of the ''cluster'' regime, the main feature remains similar for the three solvent media, and micrometer-sized clusters can be clearly identified by the SALS plateaus. The mean cluster size shown in Table 2, $R_{g,cluster}$, follows a similar trend as previously revealed by the DLS analysis, namely, DMAc and NMP foster larger clusters than does the 1 : 1 DMAc/NMP medium. The fitted parameters (G) shown in Table S1 (ESI†) also consistently exhibit a smaller contribution to the scattering intensity for the cluster species in the mixed-solvent medium. Both bearing a secondary structure, the clusters incubated in the 1 : 1 DMAc/NMP and NMP media differ primarily in the average aggregation number defined as $N_{agg} = (R_{g,cluster}/R_{g,agg})^{D_{m,cluster}}$, which yields $N_{agg} \sim 206$ and $N_{agg} \sim 412$, respectively. A much smaller N_{agg} for the 1 : 1 DMAc/NMP medium could be due to an improved solvent quality under the synergetic effects of two distinct solvents that are selectively attractive to different parts of the polyelectrolyte molecule. In fact, the ratio $\rho_{cluster} = R_{g,cluster}/R_{H,cluster}$ shown in Table 2 clearly indicates that the DMAc medium produces a cluster species that is rather compact in its interior structure (*i.e.*, a small value of ρ as reported for associating polyelectrolytes[58]), an indication of poor solvent quality.

The hierarchical structures that define a typical polyelectrolyte cluster, along with the associated polyion and aggregate species, are pictorially illustrated in Fig. 5. Our conjecture is that the presence of a secondary structure for the clusters incubated in the 1 : 1 DMAc/NMP and NMP media helps promote the mesoscale ion conduction within a cluster and, with proper cluster–cluster interactions, fulfill efficient bulk ion conduction in solution and membrane. To shed some light on this issue, we perform dielectric measurements on the same polyelectrolyte solutions as investigated above, with the results presented in Fig. 6. For the range of frequencies investigated, the dielectric responses in the low- (<0.1 Hz) and high-frequency ($>10^3$ Hz) regime might be influenced by electrode polarizations and the orientational polarization of solvent molecules, respectively.[78,79] At intermediate frequencies, the measured conductance data reflect the ac conductivity of a given polyelectrolyte solution that arises from counterion fluctuations along the polyions.[78] It can be seen that the use

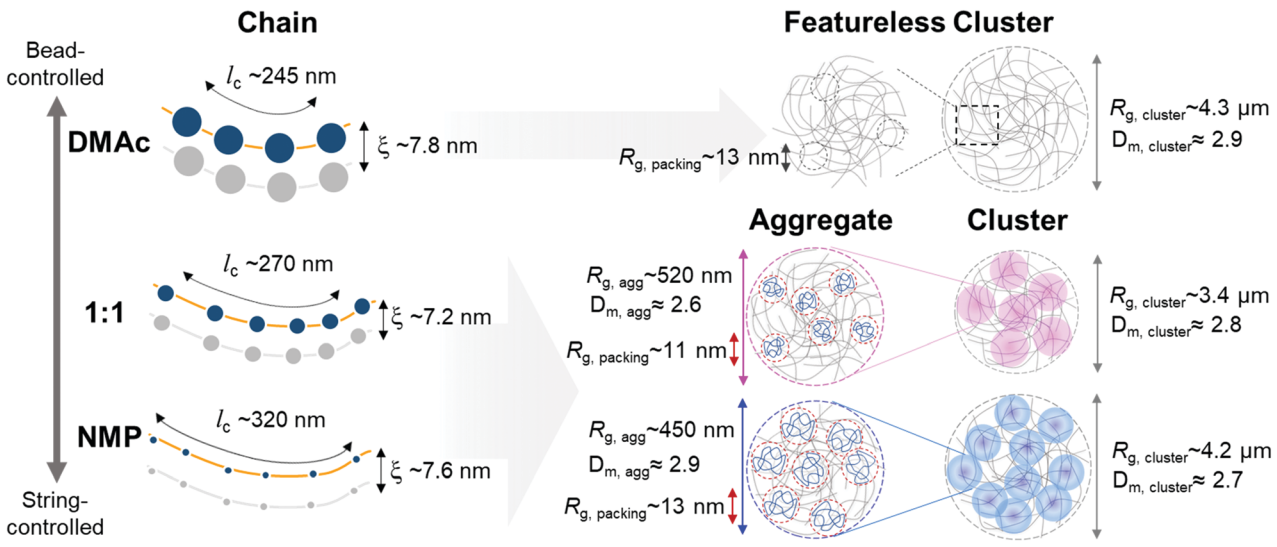

Fig. 5 Pictorial illustrations of multiscale structural features of the polyion, aggregate, and cluster species fostered in various solvent media. Note that the DMAc system lacks the aggregate species and a secondary structure and, consequently, possesses relatively homogeneous and featureless interior domains for the cluster species.

 This journal is © the Owner Societies 2019

Published on 25 January 2019. Downloaded by National Synchrotron Radiation Research on 1/9/2020 4:44:22 AM.

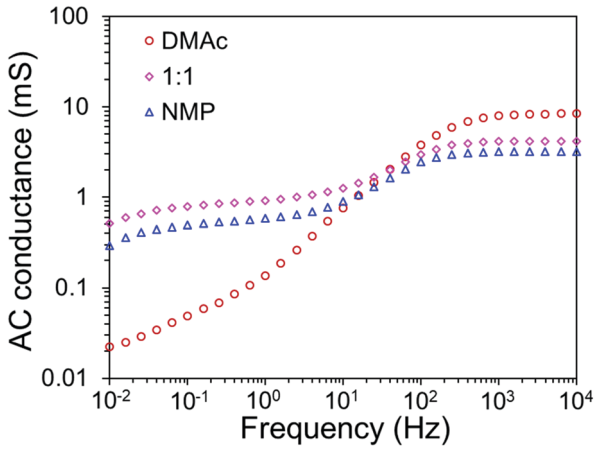

Fig. 6 Comparison of the ac conductance for the 1 wt% polyelectrolyte solutions prepared with three different solvent media as investigated in Fig. 4.

of DMAc substantially reduces the ac conductivity of the polyelectrolyte solution. In contrast, the somewhat optimal performance for the solution prepared with the 1 : 1 DMAc/NMP medium can be observed, probably due to optimized cluster properties[8] that should, in principle, include the population, size, and interior structure.

Conclusion

The solution properties of a synthesized imidazolium-based amphiphilic polyelectrolyte dissolved in a representative series of pure- and mixed-solvent media composed of two aprotic polar solvents, DMAc and NMP, having a similar dielectric constant are explored using multiscale dynamic/static analysis schemes. While DMAc is selectively attractive to the alkyl side-chain of the polyelectrolyte molecule, the other solvent NMP is attractive to the imidazolium side-chain as well as to the polymer backbone in view of structural similarity. This study suggests that the synergic effects of the mixed-solvent media may be utilized to gain further controls over the population, size, and structure of (nanometer-sized) polyion and (micrometer-sized) cluster species, rendering it possible to forge a pronounced reduction in solution viscosity and critical gel behavior ($G' \sim G'' \sim \omega^{0.5}$) that are expected to greatly facilitate the solution processing without compromising the mechanical strength of solution-cast membranes. Additionally, the cluster species incubated in the 1 : 1 DMAc/NMP and NMP media that bears hierarchical structures is believed to enhance the (mesoscale) ion conduction, as supported by ac conductivity measurements. Interestingly, the underlying physics for the mixed-solvent polyelectrolyte solutions investigated seems to represent a distinct type of reentrant transition in solvent quality (poorer-better-poorer, with increased fraction of the second solvent) as compared with the phenomena previously reported for PNIPAM in water/methanol mixtures (good-poor-good) wherein solvent complexion was resolved to play an important role.[61,62] The whole impact of solvent quality, however, cannot be readily explained by any single rule that dictates the polyion and aggregate (cluster) properties, especially when different (dynamic or static) features and (multiscale) scales are concerned. The overall findings suggest that an appropriate selection of mixed-solvent media may be utilized to promote the rheological, structural, and ion-conduction properties of a polyelectrolyte solution beyond the reach of the corresponding pure solvents. Given the scarcity of similar phenomena revealed for the solution system of an amphiphilic polymer, the underlying physics and molecular interactions await future exploration from more extensive experimental and computational studies.

Conflicts of interest

L. D. T. and M. C. C. are named inventors on a patent application related to this work.

Acknowledgements

The authors thank the supports from the Industrial Technology Research Institute of ROC and Ministry of Science and Technology of ROC (MOST 106-2221-E-194-055). We acknowledge the NSRRC of ROC for providing beamtimes and facilitating the SAXS experiments.

References

1 G. Merle, M. Wessling and K. Nijmeijer, *J. Membr. Sci.*, 2011, **377**, 1–35.
2 M. A. Hickner, A. M. Herring and E. B. Coughlin, *J. Polym. Sci., Part B: Polym. Phys.*, 2013, **51**, 1727–1735.
3 J. Ran, L. Wu, Y. He, Z. Yang, Y. Wang, C. Jiang, L. Ge, E. Bakangura and T. Xu, *J. Membr. Sci.*, 2017, **522**, 267–291.
4 Y.-J. Wang, J. Qiao, R. Baker and J. Zhang, *Chem. Soc. Rev.*, 2013, **42**, 5768–5787.
5 S. S. He, A. L. Strickler and C. W. Frank, *ChemSusChem*, 2015, **8**, 1472–1483.
6 S. Banerjee, S. Ray, S. Maiti, K. K. Sen, U. Bhattacharyya, S. Kaity and A. Ghosh, *Int. J. Appl. Pharm.*, 2010, **2**, 28–34.
7 M. Shivashankar and B. K. Mandal, *Int. J. Pharm. Pharm. Sci.*, 2012, **4**, 1–7.
8 J. Pan, C. Chen, Y. Li, L. Wang, L. Tan, G. Li, X. Tang, L. Xiao, J. Lu and L. Zhuang, *Energy Environ. Sci.*, 2014, **7**, 354–360.
9 D. Guo, A. N. Lai, C. X. Lin, Q. G. Zhang, A. M. Zhu and Q. L. Liu, *ACS Appl. Mater. Interfaces*, 2016, **8**, 25279–25288.
10 S. S. He and C. W. Frank, *J. Mater. Chem. A*, 2014, **2**, 16489–16497.
11 J. Ran, L. Wu, Q. Ge, Y. Chen and T. Xu, *J. Membr. Sci.*, 2014, **470**, 229–236.
12 E. A. Weiber and P. Jannasch, *ChemSusChem*, 2014, **7**, 2621–2630.
13 Y. He, L. Wu, J. Pan, Y. Zhu, X. Ge, Z. Yang, J. Ran and T. Xu, *J. Membr. Sci.*, 2016, **504**, 47–54.

Published on 25 January 2019. Downloaded by National Synchrotron Radiation Research on 1/9/2020 4:44:22 AM.

14 J. Pan, L. Zhu, J. Han and M. A. Hickner, *Chem. Mater.*, 2015, **27**, 6689–6698.
15 D. Guo, Y. Z. Zhuo, A. N. Lai, Q. G. Zhang, A. M. Zhu and Q. L. Liu, *J. Membr. Sci.*, 2016, **518**, 295–304.
16 A. N. Lai, D. Guo, C. X. Lin, Q. G. Zhang, A. M. Zhu, M. L. Ye and Q. L. Liu, *J. Power Sources*, 2016, **327**, 56–66.
17 M. Tanaka, K. Fukasawa, E. Nishino, S. Yamaguchi, K. Yamada, H. Tanaka, B. Bae, K. Miyatake and M. Watanabe, *J. Am. Chem. Soc.*, 2011, **133**, 10646–10654.
18 Y. He, J. Si, L. Wu, S. Chen, Y. Zhu, J. Pan, X. Ge, Z. Yang and T. Xu, *J. Membr. Sci.*, 2016, **515**, 189–195.
19 L. Liu, X. Chu, J. Liao, Y. Huang, Y. Li, Z. Ge, M. A. Hickner and N. Li, *Energy Environ. Sci.*, 2018, **11**, 435–446.
20 D. Dong, X. Wei, J. B. Hooper, H. Pan and D. Bedrov, *Phys. Chem. Chem. Phys.*, 2018, **20**, 19350–19362.
21 M. A. Vandiver, B. R. Caire, T. P. Pandey, Y. Li, S. Seifert, A. Kusoglu, D. M. Knauss, A. M. Herring and M. W. Liberatore, *J. Membr. Sci.*, 2016, **497**, 67–76.
22 H. A. Kostalik, T. J. Clark, N. J. Robertson, P. F. Mutolo, J. M. Longo, H. D. Abruña and G. W. Coates, *Macromolecules*, 2010, **43**, 7147–7150.
23 K. J. T. Noonan, K. M. Hugar, H. A. Kostalik, E. B. Lobkovsky, H. D. Abruña and G. W. Coates, *J. Am. Chem. Soc.*, 2012, **134**, 18161–18164.
24 T.-H. Tsai, S. P. Ertem, A. M. Maes, S. Seifert, A. M. Herring and E. B. Coughlin, *Macromolecules*, 2015, **48**, 655–662.
25 M. Zhang, H. K. Kim, E. Chalkova, F. Mark, S. N. Lvov and T. C. M. Chung, *Macromolecules*, 2011, **44**, 5937–5946.
26 S. P. Ertem, T.-H. Tsai, M. M. Donahue, W. Zhang, H. Sarode, Y. Liu, S. Seifert, A. M. Herring and E. B. Coughlin, *Macromolecules*, 2016, **49**, 153–161.
27 A. C. Tibbits, L. E. Mumper, C. J. Kloxin and Y. S. Yan, *J. Electrochem. Soc.*, 2015, **162**, F1206–F1211.
28 J. Won, Y. S. Kang, H. C. Park and U. Y. Kim, *J. Membr. Sci.*, 1998, **145**, 45–52.
29 Y. Amamoto, H. Otsuka, A. Takahara and K. Matyjaszewski, *ACS Macro Lett.*, 2012, **1**, 478–481.
30 K. J. Henderson and K. R. Shull, *Macromolecules*, 2012, **45**, 1631–1635.
31 L. Ghimici, M. Nichifor and B. Wolf, *J. Phys. Chem. B*, 2009, **113**, 8020–8025.
32 A.-H. Vesterinen, J. Rich and J. Seppälä, *J. Colloid Interface Sci.*, 2010, **351**, 478–484.
33 W. Essafi, W. Raissi, A. Abdelli and F. Boué, *J. Phys. Chem. B*, 2014, **118**, 12271–12281.
34 P. Loh, G. R. Deen, D. Vollmer, K. Fischer, M. Schmidt, A. Kundagrami and M. Muthukumar, *Macromolecules*, 2008, **41**, 9352–9358.
35 W. Essafi, M.-N. Spiteri, C. Williams and F. Boue, *Macromolecules*, 2009, **42**, 9568–9580.
36 W. Essafi, A. Abdelli, G. Bouajila and F. Boué, *J. Phys. Chem. B*, 2012, **116**, 13525–13537.
37 W. Essafi, N. Haboubi, C. Williams and F. Boué, *J. Phys. Chem. B*, 2011, **115**, 8951–8960.
38 M. N. Spiteri, C. E. Williams and F. Boué, *Macromolecules*, 2007, **40**, 6679–6691.
39 C.-T. Wang, L.-D. Tsai, C.-H. Tsai, C.-H. Su and M.-C. Chen, *US Pat.*, 15/135851, 2017.
40 Y. H. Wen, P. C. Lin, C. C. Hua and S. A. Chen, *J. Phys. Chem. B*, 2011, **115**, 14369–14380.
41 R. H. Guo, C. H. Hsu, C. C. Hua and S. A. Chen, *J. Phys. Chem. B*, 2015, **119**, 3320–3331.
42 H. L. Yi, C. H. Wu, C. I. Wang and C. C. Hua, *Macromolecules*, 2017, **50**, 5498–5509.
43 A. Pal and R. K. Bhardwaj, *J. Chem. Eng. Data*, 2002, **47**, 1128–1134.
44 C. Yang, W. Xu and P. Ma, *J. Chem. Eng. Data*, 2004, **49**, 1794–1801.
45 Q. Pu and S. B. Chen, *Langmuir*, 2003, **19**, 4034–4036.
46 H. H. Winter and F. Chambon, *J. Rheol.*, 1986, **30**, 367–382.
47 T. A. Waigh, R. Ober, C. E. Williams and J.-C. Galin, *Macromolecules*, 2001, **34**, 1973–1980.
48 K. Nishi, S. Tochioka, T. Hiroi, T. Yamada, K. Kokado, T.-H. Kim, E. P. Gilbert, K. Sada and M. Shibayama, *Macromolecules*, 2015, **48**, 3613–3621.
49 T. M. Aminabhavi and B. Gopalakrishna, *J. Chem. Eng. Data*, 1995, **40**, 856–861.
50 J. George and N. V. Sastry, *J. Chem. Eng. Data*, 2004, **49**, 235–242.
51 M. Sedlák, *Langmuir*, 1999, **15**, 4045–4051.
52 Z. Cao and G. Zhang, *Polymer*, 2014, **55**, 6789–6794.
53 M. Sedlák, *J. Chem. Phys.*, 1997, **107**, 10799–10804.
54 B. D. Ermi and E. J. Amis, *Macromolecules*, 1998, **31**, 7378–7384.
55 M. Sedlák, *J. Chem. Phys.*, 2002, **116**, 5256–5262.
56 H. Nie, M. Li, R. Bansil, Č. Koňák, M. Helmstedt and J. Lal, *Polymer*, 2004, **45**, 8791–8799.
57 C. Konak, G. Fleischer, Z. Tuzar and R. Bansil, *J. Polym. Sci., Part B: Polym. Phys.*, 2000, **38**, 1312–1322.
58 E. V. Korchagina and O. E. Philippova, *Biomacromolecules*, 2010, **11**, 3457–3466.
59 A. Y. Grosberg and A. R. Khokhlov, *Statistical Physics of Macromolecules*, AIP Press, New York, 1994.
60 S. K. Filippov, A. V. Lezov, O. Y. Sergeeva, A. S. Olifirenko, S. B. Lesnichin, N. S. Domnina, E. A. Komarova, M. Almgren, G. Karlsson and P. Štepanek, *Eur. Polym. J.*, 2008, **44**, 3361–3369.
61 G. Zhang and C. Wu, *Phys. Rev. Lett.*, 2001, **86**, 822–825.
62 G. Zhang and C. Wu, *J. Am. Chem. Soc.*, 2001, **123**, 1376–1380.
63 C. K. Lee, C. C. Hua and S. A. Chen, *Macromolecules*, 2011, **44**, 320–324.
64 L. Liu, T. Wang, C. Liu, K. Lin, Y. Ding, G. Liu and G. Zhang, *J. Phys. Chem. B*, 2013, **117**, 2535–2544.
65 M.-C. Chen, W.-C. Hung, A.-C. Su, S.-H. Chen and S.-A. Chen, *J. Phys. Chem. B*, 2009, **113**, 11124–11133.
66 M. Zheng, F. Bai and D. Zhu, *J. Photochem. Photobiol., A*, 1998, **116**, 143–145.
67 U.-S. Jeng, C. H. Su, C.-J. Su, K.-F. Liao, W.-T. Chuang, Y.-H. Lai, J.-W. Chang, Y.-J. Chen, Y.-S. Huang, M.-T. Lee, K.-L. Yu, J.-M. Lin, D.-G. Liu, C.-F. Chang, C.-Y. Liu, C.-H. Chang and K. S. Liang, *J. Appl. Crystallogr.*, 2010, **43**, 110–121.
68 E. Josef and H. Bianco-Peled, *Soft Matter*, 2012, **8**, 9156–9165.

 This journal is © the Owner Societies 2019

Published on 25 January 2019. Downloaded by National Synchrotron Radiation Research on 1/9/2020 4:44:22 AM.

69 E. Buhler and F. Boué, *Macromolecules*, 2004, **37**, 1600–1610.
70 J. Combet, P. Lorchat and M. Rawiso, *Eur. Phys. J.-Spec. Top.*, 2012, **213**, 243–265.
71 B. Hammouda, *J. Appl. Crystallogr.*, 2010, **43**, 716–719.
72 P. Sharp and V. A. Bloomfield, *Biopolymers*, 1968, **6**, 1201–1211.
73 S. W. Cranford and M. J. Buehler, *Macromolecules*, 2012, **45**, 8067–8082.
74 M. Muthukumar, *Macromolecules*, 2017, **50**, 9528–9560.
75 S. Popa-Nita, C. Rochas, L. David and A. Domard, *Langmuir*, 2009, **25**, 6460–6468.
76 A. V. Dobrynin, M. Rubinstein and S. P. Obukhov, *Macromolecules*, 1996, **29**, 2974–2979.
77 Y. S. Vygodskii, A. S. Shaplov, E. I. Lozinskaya, K. A. Lyssenko, D. G. Golovanov, I. A. Malyshkina, N. D. Gavrilova and M. R. Buchmeiser, *Macromol. Chem. Phys.*, 2008, **209**, 40–51.
78 F. Bordi, C. Cametti, T. Gili, S. Sennato, S. Zuzzi, S. Dou and R. H. Colby, *Phys. Rev. E: Stat., Nonlinear, Soft Matter Phys.*, 2005, **72**, 031806.
79 F. Bordi, C. Cametti, S. Sennato, S. Zuzzi, S. Dou and R. H. Colby, *Phys. Chem. Chem. Phys.*, 2006, **8**, 3653–3658.